Shape isometric states in heavy nuclei

Nilsson, Sven Gösta; Tsang, Chin Fu

Published in:
Nuclear Physics, Section A

1970

2.M *Nuclear Physics* A140 (1970) 275—288; © *North-Holland Publishing Co., Amsterdam*

SHAPE ISOMERIC STATES IN HEAVY NUCLEI

CHIN FU TSANG and SVEN GÖSTA NILSSON †
Lawrence Radiation Laboratory ††, *University of California, Berkeley, California 94720*

Received 3 October 1969

Abstract: The trend for the occurrence of secondary minima (shape isomers) in the potential-energy surface is discussed for an extended region of heavy nuclei. The calculations reported are based on a modified oscillator potential, and a renormalization of the average behaviour of the total energy to that of the liquid-drop model is performed. The regions treated are the actinide region, the rare-earth region along the stability line, and a region of neutron deficient isotopes of elements in the Pb region.

1. Introduction

The fission isomers were first discovered in the experiments of Polikanov, Flerov *et al.* [1,2]), and they have been studied extensively in more recent experiments [3]). Several attempts have been made to identify them with the shape isomeric state corresponding to a secondary minimum largely along the axis of quadrupole distortions that has been found to occur in the total potential-energy surface plotted as a function of deformations. Thus instead of the conventional picture of a one-peaked energy barrier along the deformation path leading to fission, one has a two-peaked barrier, where between the two peaks there is a secondary minimum at a higher energy than the ground state minimum but hindered in its decay to the ground state or fission by the two potential energy peaks.

Probably the first of the attempts to theoretically locate the minimum in this part of the potential-energy surface are the early publications of Strutinsky [4]) and Gustafson *et al.* [5]). The first paper introduces the new and very fruitful idea of the renormalization of the total single-particle energy to the liquid-drop model by a method sometimes cited as the "Strutinsky Prescription". The purpose of the procedure quoted is to correct for the somewhat improper behaviour of the total single-particle energy calculated by the conventional recipes at very large distortions, and it has been the method employed in all relevant subsequent calculations of the fission barrier based on the single-particle model. To describe the liquid-drop energy this paper employed an expansion in the deformation parameter ε, which has a poor convergence so that the second peak of the two-peaked barrier is somewhat suppressed. In the second paper [5]), which employed a much improved single-particle potential, a weak

† On leave of absence from Lund Institute of Technology, Lund, Sweden.
†† Work performed under the auspices of the U. S. Atomic Energy Commission.

secondary minimum can be found for a series of nucleides at about the right distortion. For computational reasons the calculation was only carried so far in distortion as to the beginning of the second peak †. This latter paper [5]) is based on the modified oscillator model without renormalization to the liquid drop model.

2. Present method of calculations

The single-particle potential used in ref. [5]) has been employed in the much more realistic and more successful subsequent calculations by Nilsson *et al.* [6,7]). (This work is paralleled by the publications of the Strutinsky group [8,9]).) In all of these references the Strutinsky prescription is employed. Two degrees of freedom are considered: P_2 and P_4 distortions, measured by the coordinates ε and ε_4. Oblate and prolate shapes are represented by negative and positive ε-values, respectively. The sign of ε_4 is so defined that a positive ε_4 represents a waistline indentation relative to the spheroid shape defined by ε. The potential is given as

$$V = \tfrac{1}{2}\hbar\omega_0(\varepsilon, \varepsilon_4)\rho^2(1-\tfrac{2}{3}\varepsilon P_2+\varepsilon_4 P_4)+(\boldsymbol{l}\cdot\boldsymbol{s} \text{ and } \boldsymbol{l}^2) \text{ terms},$$

where ρ is the radius vector length in so-called stretched coordinates [6]). In recent calculations [10,11]) also P_3 and P_6 shapes have been considered in addition to the gamma (rotationally asymmetric) degree of freedom [12]). However the ε and ε_4 coordinates presently appear to be the most relevant ones for the barrier penetration problem.

In these calculations, in accordance with the Strutinsky prescription, the averaged energy is subtracted out from the sum of the single-particle energies. The remaining energy is referred to as "the shell contribution". To this energy is then added the surface and Coulomb energy terms in the liquid-drop model with parameters taken from the papers of Myers and Swiatecki [13]). The Coulomb energy term is evaluated numerically employing a method due to Nix [14]). Pairing energy is also added, in which a surface and isospin dependent pairing matrix element is introduced [7]). In this way the total potential-energy surface is calculated as a function of deformations. Strutinsky, Muzychka and co-workers [15]) have also calculated the potential energy by a similar method. However, in their work the P_4 deformation is neglected and, so far, their calculations have been restricted to the regions of actinide and superheavy nuclei.

3. The potential energy surface

In figs. 1–6 the potential energy surfaces in the $(\varepsilon, \varepsilon_4)$ plane are shown for ^{228}U, ^{242}Pu, ^{244}Cm, ^{250}Cf, ^{252}Fm and ^{254}No. One way to exhibit the fission barrier is to plot the potential energy as a function of ε with minimization of energy with respect to ε_4 for each value of ε. This type of plot represents a cut through the two-dimensional potential surface along the potential energy minimum path with the energies projected on the ε axis.

† In the region near $A \approx 195$ the secondary minimum is particularly apparent in these calculations.

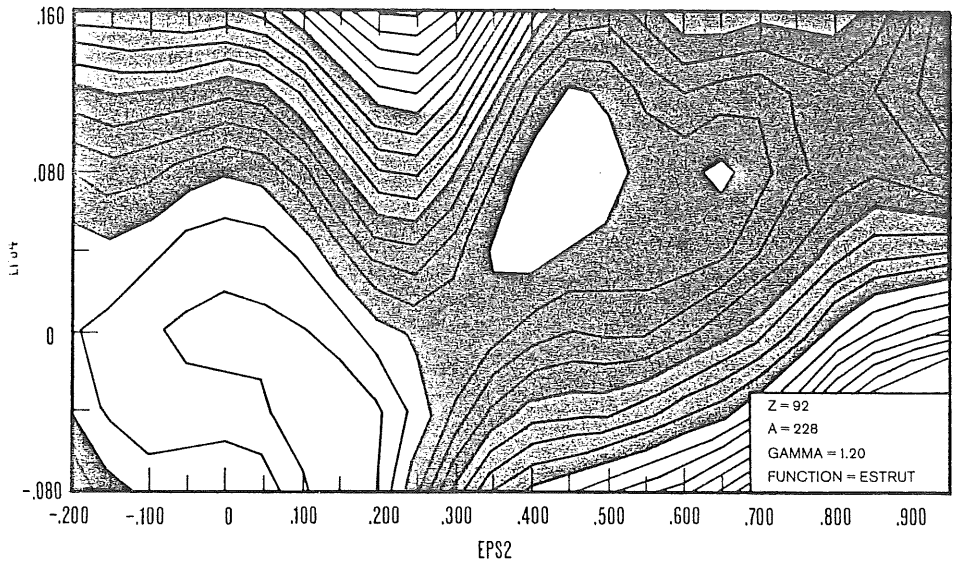

Fig. 1. Total potential-energy surface of ^{228}U given as a contour map in (ε, ε_4) plane [7]). The contour lines represent steps of 1 MeV.

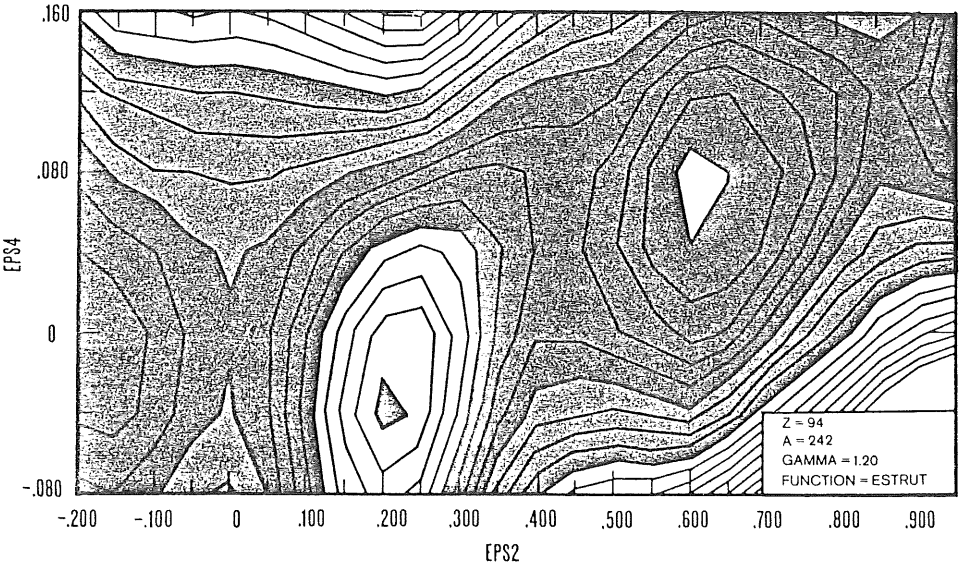

Fig. 2. Same as fig. 1 for ^{242}Pu.

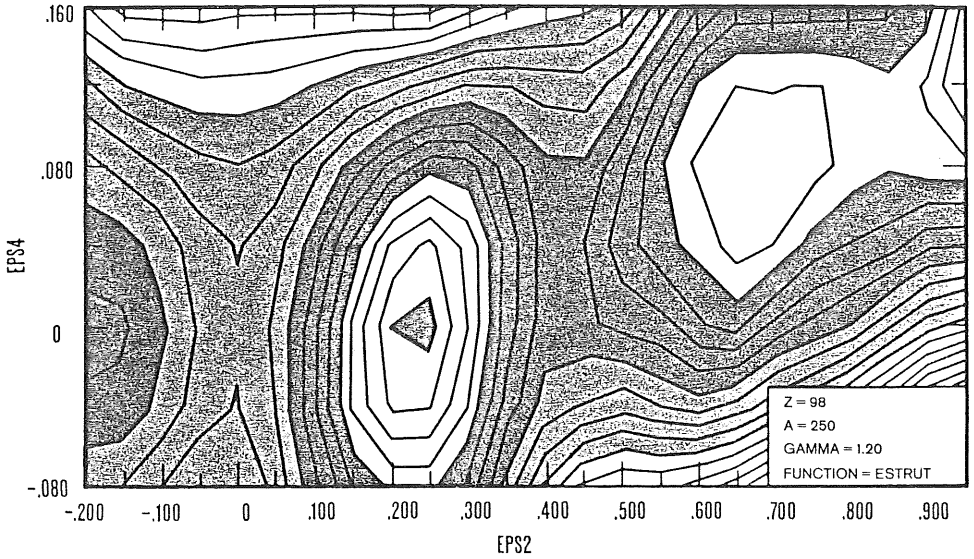

Fig. 4. Same as fig. 1 for ^{250}Cf.

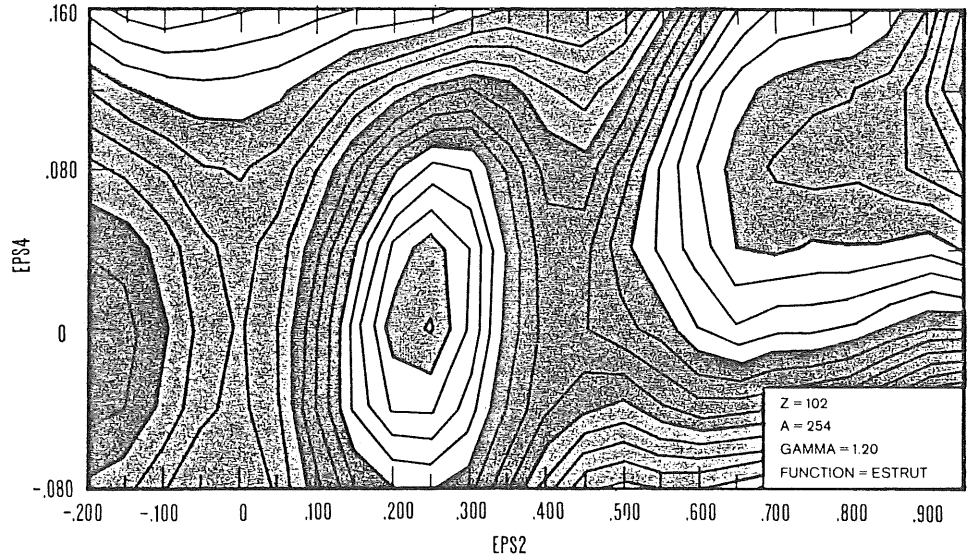

Fig. 6. Same as fig. 1 for ^{254}No.

In fig. 7 we show such a plot for the superheavy nucleides $^{298}114$ and $^{294}110$ and two actinide nucleides $^{242}94$ and $^{254}100$. From the figure we see that for a nucleus with its proton or neutron number near a magic number the ground state is spherical, ($\varepsilon = 0$), but a secondary minimum occurs at $\varepsilon \approx 0.4$. For a nucleus with its neutron

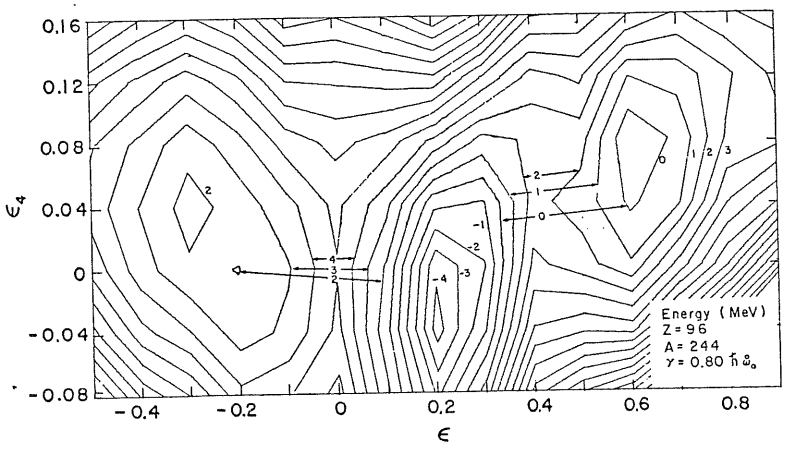

Fig. 3. Same as fig. 1 for ^{244}Cm.

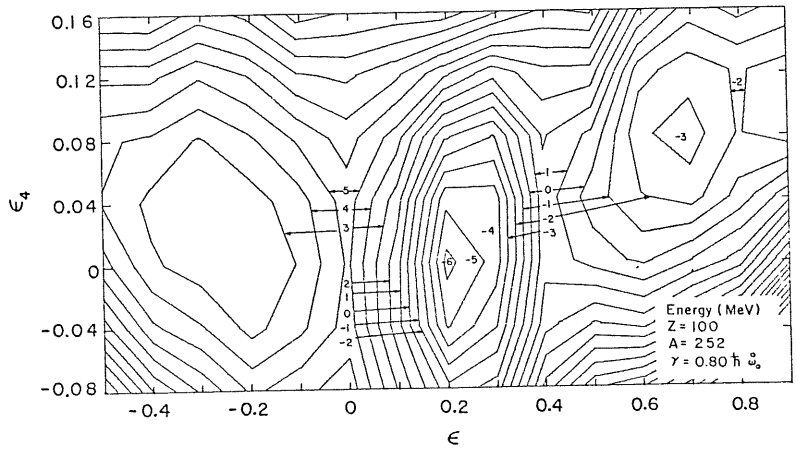

Fig. 5. Same as fig. 1 for ^{252}Fm.

and proton numbers away from the magic numbers the ground state occurs at $\varepsilon \approx 0.2-0.25$ and a secondary minimum occurs at $\varepsilon \approx 0.6-0.7$.

The existence of the two-peak structure of the potential-energy barrier is sometimes described as due to a "secondary shell effect", the "primary shell effect" being responsible for the ground state deformations. If this effect occurs at or near the liquid-drop saddle point, the peaks will be of about equal height.

For lighter nuclei with small fissility, x, i.e. large liquid-drop fission barriers, also a "ternary shell effect" may occur. However, in particular due to the damping effect of the pairing matrix element G, assumed proportional to the surface area, the shell fluctuations may be expected to decrease in amplitude with distortion.

The secondary minimum is found to occur in the region of deformation $\varepsilon = 0.35$ to 0.75 depending on the N and Z values of the nucleus considered. As we go along the stability line in the periodic table from small-A to large-A nuclei, the fissility parameter x increases and the liquid-drop saddle point region will move from large ε to small ε. For the rare-earth region near beta stability the liquid-drop saddle

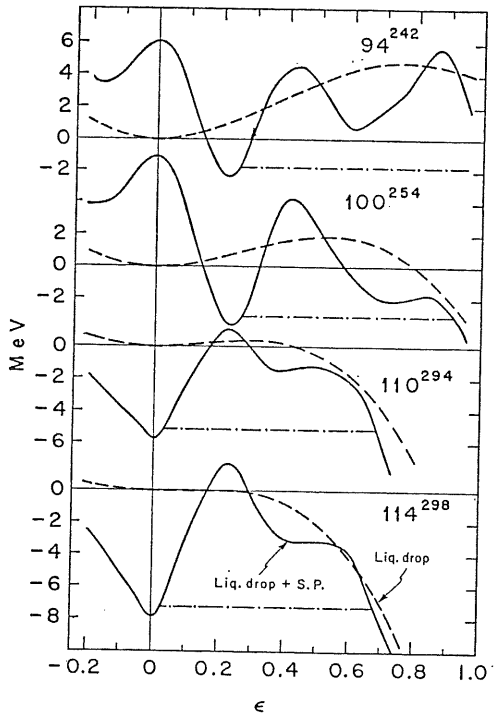

Fig. 7. Potential energy (solid curve) minimized with respect to ε_4 as functions of ε for various nuclei to illustrate the shell structure effects in relation to the liquid-drop background (dashed curve).

points are located beyond $\varepsilon = 1.0$, whereas in the actinide region they are located between $\varepsilon \approx 0.5$ and $\varepsilon \approx 0.9$. Thus it appears reasonable that the two-peaked structure in the fission barrier is particularly prominent in the actinide region. Another favourable region with similar x-values is that of neutron deficient nucleides with $Z \approx 82$.

4. Shape (fission) isomers in the actinide region

Fission isomers have long been observed and studied in the actinide region. In this region the corresponding single-particle graphs are available and provide a more detailed understanding of the relation between the shell crossings and the occurrence of the peaks and valleys in the fission barrier. If we follow along the Fermi level corresponding to, for instance, $N = 150$ or $Z = 100$ in figures 2k and 2l of ref. [7]), we notice the following. The first strongly downward trend in the potential-energy

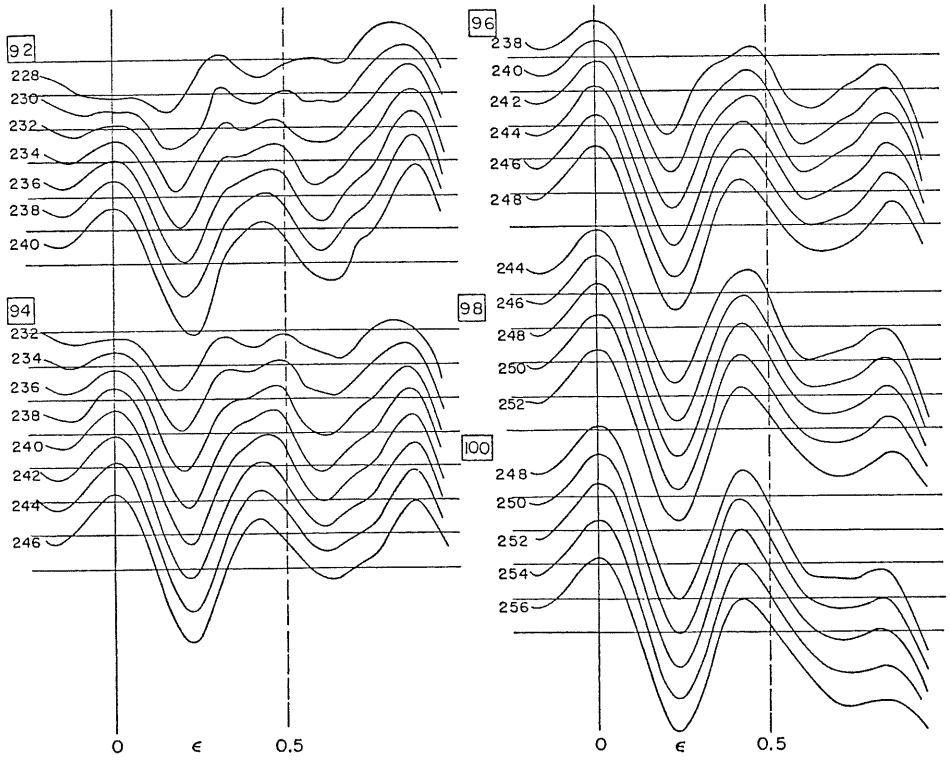

Fig. 8. The projected two-peak barrier as function of mass number for $Z = 92-100$ (see ref. [7])).

surface along the axis of P_2 distortion (the ε-axis) is caused by the crossing of shells with $\Delta N = 1(2)$, where the figure in parenthesis refers to states from subshells pulled down by the spin-orbit force from the next shell above. After this the energy surface again obtains a positive second derivative due to the volume conservation of the harmonic-oscillator potential well. Thereby the first minimum, situated at about $\varepsilon \simeq 0.25$, is formed. The next downward trend is caused by shell crossings with $\Delta N = 2(3)$ followed by a secondary minimum in the relative absence of more cross-

ings. This occurs at about $\varepsilon \approx 0.6-0.7$. Beyond that the second peak rises until the $\Delta N = 3(4)$ crossing in combination with the general liquid-drop energy fall-off again causes a downward trend in the actinide region. For a region of somewhat smaller x a third minimum may occur.

In fig. 8 the barriers obtained for isotopes of $Z = 92$ to $Z = 100$ can be studied with the above general discussion in mind. This figure is based on a later calculation than some of those for figs. 1–6, representing minor improvements of the theory [7]). As explained in ref. [7]) these barrier shapes are reasonably reliable for small deformation ε. For large deformations in ε (say $\varepsilon \gtrapprox 0.8$) the potential barrier is over-estimated

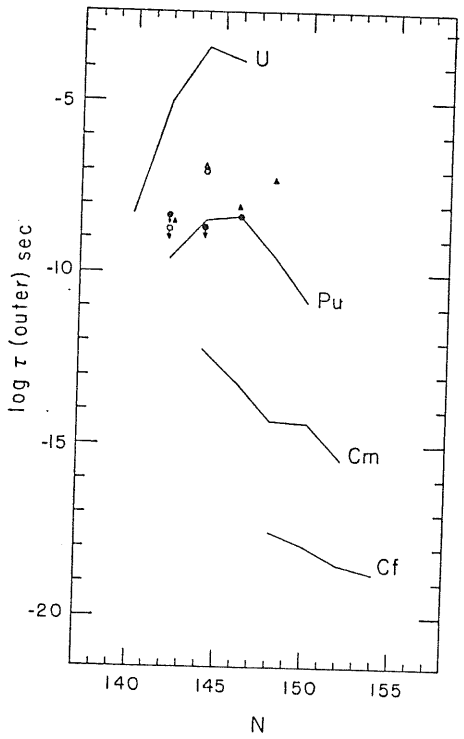

Fig. 9. Theoretical half-lives (solid curves) for fission barrier penetration of the outer peak. Experimental spontaneous fission half-lives of U isomers are shown as open triangles [3]) and circles [22]) and those of Pu isomers are shown as filled triangles [3]) and circles [22]).

mainly because of our restricted parametrization of the shape. The general trends in the figure should be noted. It is in the region of Pu and Cm, whose liquid-drop saddle points are coincident with the occurrence of the secondary shell effect, that the two-peak barrier is most prominent.

In fig. 9 we exhibit theoretical half-lives for fission decay through the outer barrier peak. These half-lives have been computed in the following way. An effective experimental inertial mass parameter B_{eff} is calculated by employing the *empirical*

ground state half-lives and our *calculated* barriers $W(\varepsilon)$ according to the relation

$$\tau_{\frac{1}{2}} \sim \exp\left[\frac{2}{\hbar}\sqrt{2B_{\text{eff}}}\int\sqrt{W(\varepsilon)-E}\,\mathrm{d}\varepsilon\right],$$

where E is the zero point energy taken to have a nominal value of $\frac{1}{2}$ MeV; where thus an effective B-value is brought outside of the integral. This same B_{eff}-value is then used to calculate the half-life for the penetration through the second barrier.

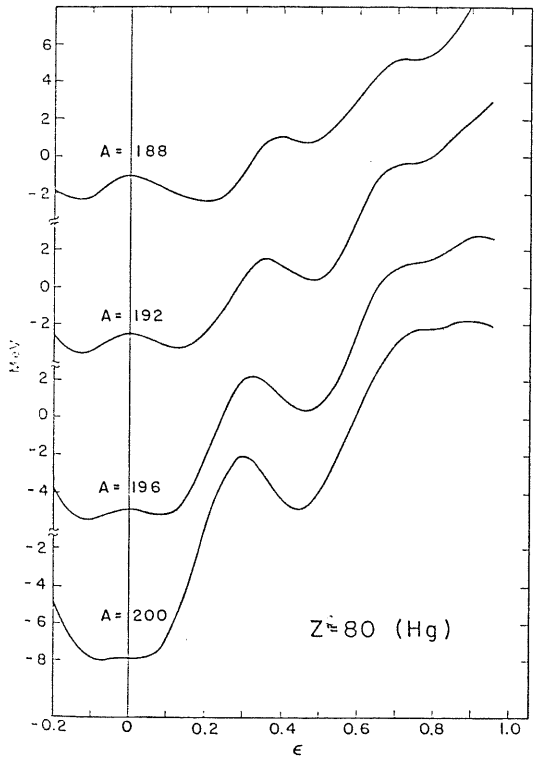

Fig. 10. Total potential energy minimized with respect to ε_4 for each ε as function of ε for *neutron deficient* isotopes of $_{80}$Hg. Calculations correspond to the assumption that the pairing strength is proportional to the nuclear surface area.

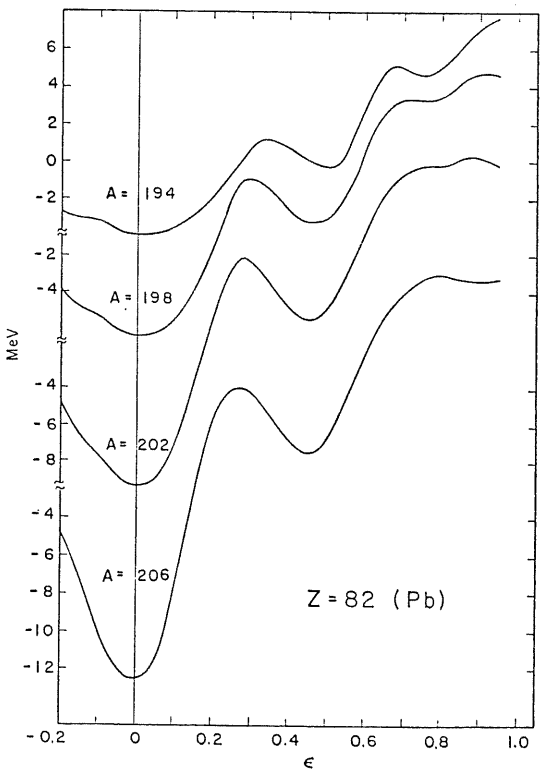

Fig. 11. Same as fig. 10 for *neutron deficient* isotopes of $_{82}$Pb.

In all likelihood this procedure underestimates the effective B-value for the penetration through the second barrier, as the microscopic calculations by Sobiczewski *et al.* [16]) bear out. We have also tried to use rB_{eff} as the inertial parameter for the penetration through the second barrier, where r is an adjustable constant. It turns out that the average value of r is approximately unity over the whole actinide region. What this means is that on the average the underestimate of our effective B value is

largely compensated for by the theoretical overestimate of the outer peak. [Recent calculations indicate a 1–2 MeV reduction of the second barrier due to the instability to P_3+P_5 distortions (P. Möller, private communication).] However for $_{92}$U, where the barrier extends to very large deformations, the overestimate of the outer barrier is not compensated by the employment of the averaged empirical inertial parameter. It is thus not surprising to find the theoretical half-lives of U isotopes somewhat too long when compared with experimental values, as is indicated in the figure. On the other hand, the barriers of Pu, Cm, Cf and Fm extend to relatively

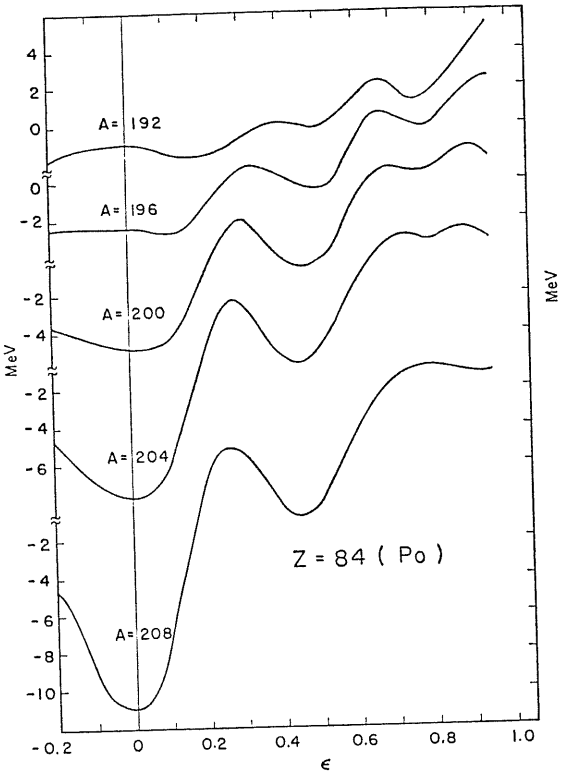

Fig. 12. Same as fig. 10 for *neutron deficient* isotopes of $_{84}$Po.

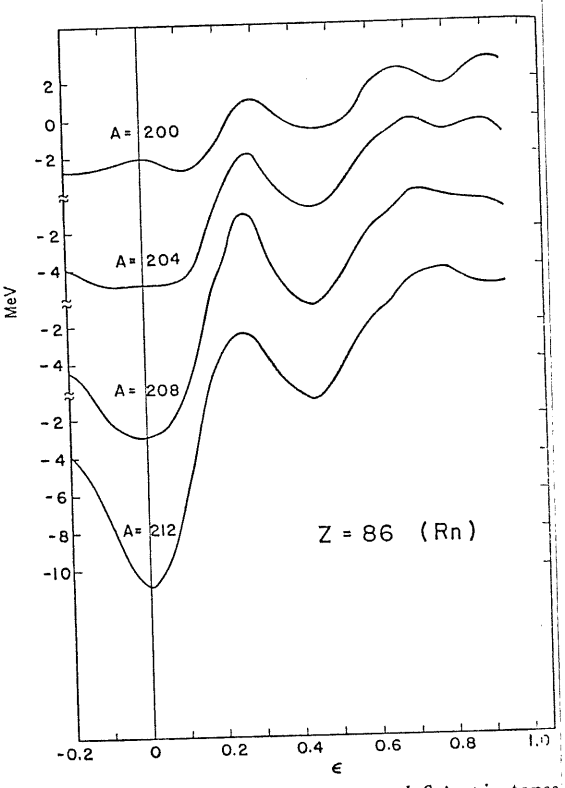

Fig. 13. Same as fig. 10 for *neutron deficient* isotopes of $_{86}$Rn.

small deformations and one would hope the estimates to be more reliable in those cases. Assuming that the theoretical calculations provide with some reliance the main trends with Z and A, this figure gives a strong indication that it is very unlikely to observe the shape fission isomers in the doubly even nuclei beyond Pu and Cm. The reported [refs. [17,18])] fission isomer case of ^{246}Cf is not verified by more recent experiments [ref. [19])].

The half-lives for penetration through the inner peak is, in many cases, shorter than those through the outer peak. However in almost all the cases the "subsequent"

gamma-decay process is probably decisive for the actual half-lives for the mode of decay involving the inner barrier.

Besides the comparison of our theoretical fission half-lives to the experimental values, one could also look at the isomer excitation energies and the barrier heights. In the cases where comparison of the excitation energy can be made, the agreement is remarkable, as shown by Lark and co-workers [3]). The highest barrier peak in the heaviest actinides is also approximately reproduced as shown in the same reference.

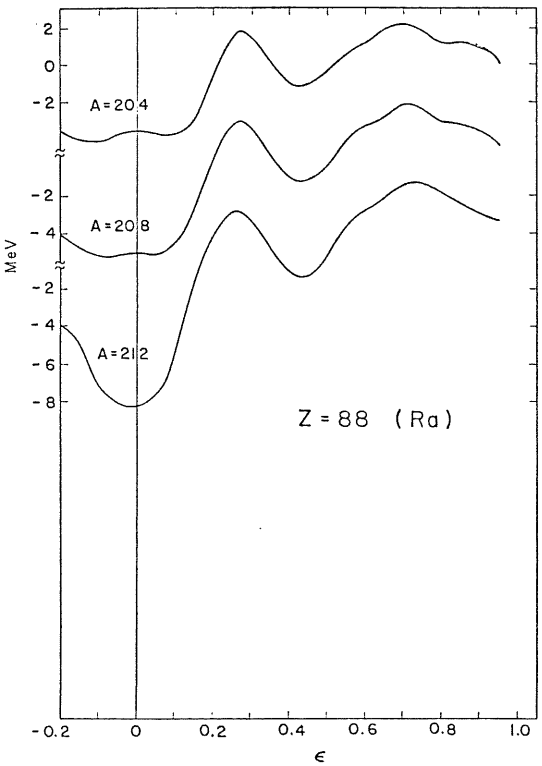

Fig. 14. Same as fig. 10 for *neutron deficient* isotopes of $_{88}$Ra.

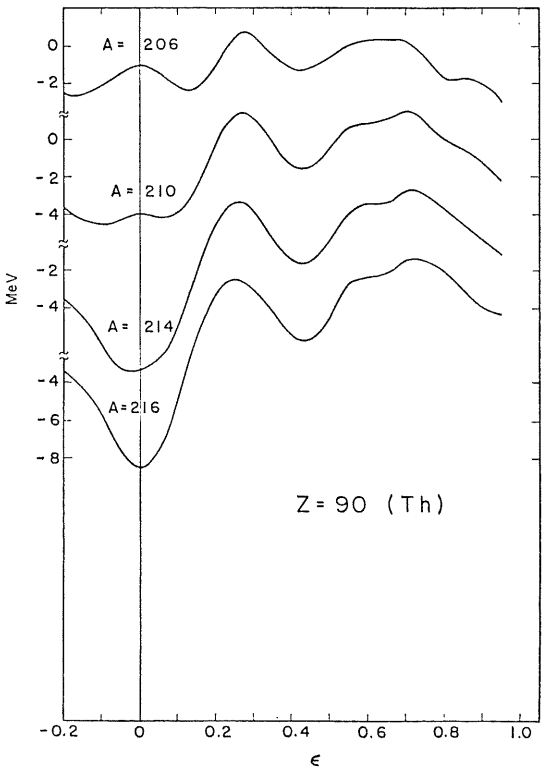

Fig. 15. Same as fig. 10 for *neutron deficient* isotopes of $_{90}$Th.

5. Shape (fission) isomers in the neutron-deficient region with $N \lesssim 126$

In figs. 10–15 we exhibit our calculated fission barriers for neutron deficient isotopes of $_{80}$Hg, $_{82}$Pb, $_{84}$Po, $_{86}$Rn, $_{88}$Ra and $_{90}$Th. It appears from these barrier shapes that the shape isomeric state would probably favor penetration through the small inner peak and subsequent gamma-decay to the ground state rather than fissioning through the much larger outer peak. Recently it is reported [20]) that fission isomers are detected in this region. An explanation may be as below.

Although the half-life for penetration through the inner peak can be estimated to

be so short compared with that for the penetration through the second peak, the subsequent gamma decay process will determine the half-life of transition back into the ground state. This in turn depends on the detailed microscopic character of the collective fission state. A considerable delay may be expected which might possibly make the fission decay through the outer barrier competitive. Furthermore we have overestimated the outer peak due to insufficient parametrization. Thus while the parametrization error in the liquid-drop part of the calculation is negligible at $\varepsilon \leqq 0.6$, it grows to nearly one MeV already at $\varepsilon \approx 0.85$. Until corrections have been made for this overestimate of the outer fission peak and until microscopic inertial mass parameters are available, we are forced to refrain from detailed quantitative estimates of the shape isomeric half-lives in this region.

6. Shape isomers along the stability line with $70 < Z < 90$

Extensive calculations of energy surfaces out to very large distortions have been performed by us down to $Z = 62$ for elements in the vicinity of the stability line. For the lighter of these the fissility parameter x is very small and consequently the

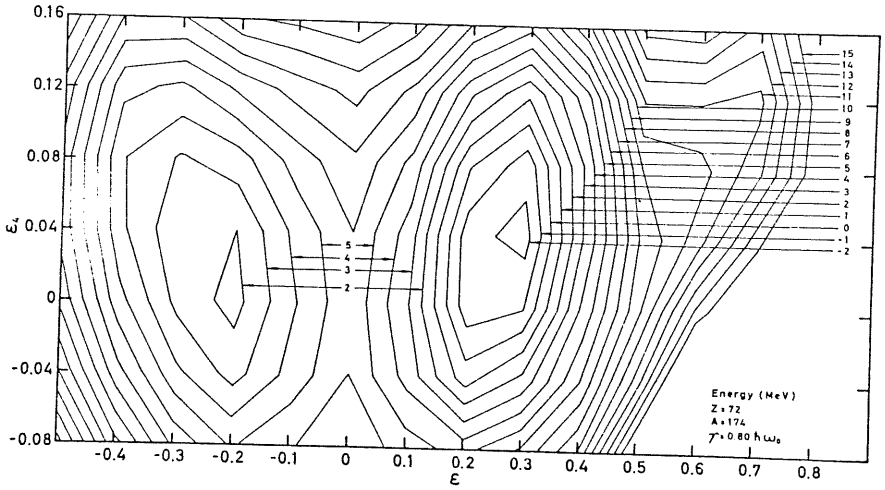

Fig. 16. Potential-energy plot in $(\varepsilon, \varepsilon_4)$ planes for ^{174}Hf. This plot corresponds to an earlier calculation of ref. [7]), where only second-order corrections to the Strutinsky smearing function have been applied.

liquid-drop barrier high and wide. Even though the shell contribution shows considerable fluctuations as a function of distortion, a real secondary minimum does not develop until about $Z = 72$ (fig. 16). Here the surface merely flattens out at an excitation of approximately 12 MeV and over a region around $\varepsilon \approx 0.6$, $\varepsilon_4 \approx 0.08$. (Note that along the ε-axis there is nc trace of an isomeric state at all to be found.)

In fig. 17 ($Z = 76$, $A = 192$) there occurs a secondary minimum at $\varepsilon = 0.4$ and at an excitation energy of about 6 MeV. For $Z = 76$, $A = 198$, a somewhat neutron rich isotope of the same element (smaller x-value) with a spherical ground state

shape, the same secondary minimum shows up at 9 MeV of excitation (fig. 18). A very deep secondary minimum occurs at about 11 MeV of excitation in ^{202}Hg (Z = 80, A = 202), fig. 19. This should constitute a long-lived gamma isomer. The low

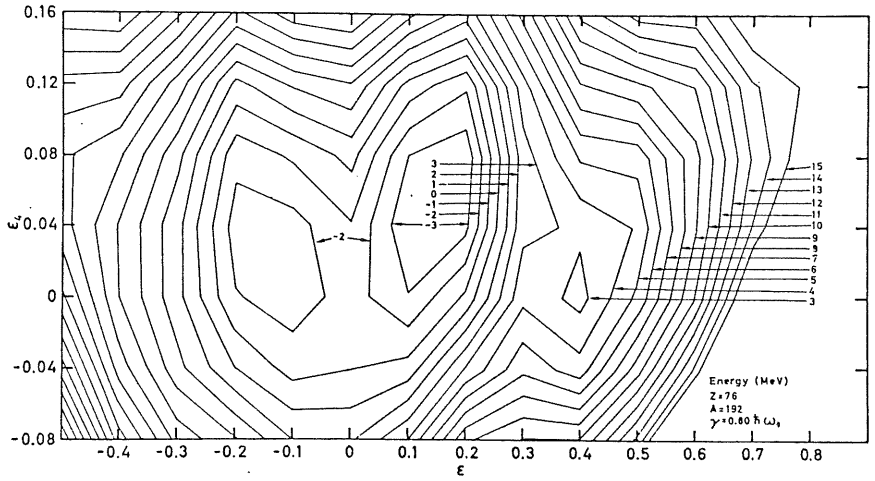

Fig. 17. Same as fig. 16 for ^{192}Os.

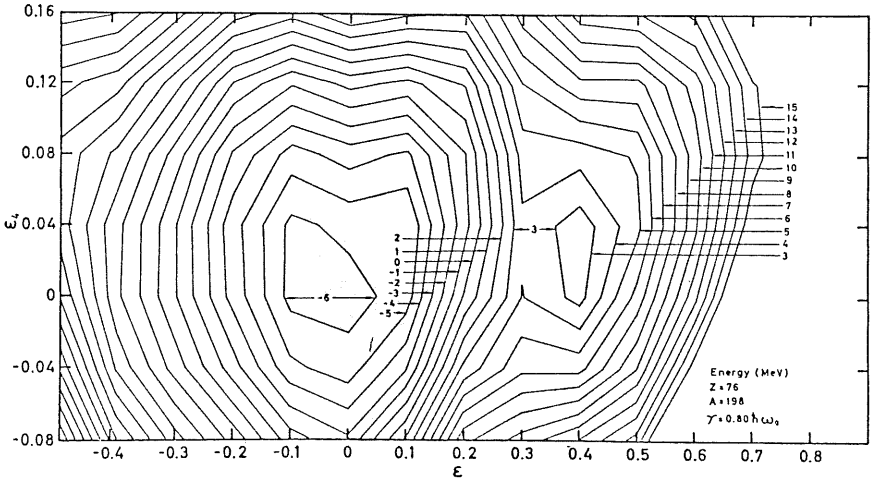

Fig. 18. Same as fig. 16 for ^{198}Os.

side of the barrier is deep enough, $\approx$ 3 MeV, to contain high-spin members of occurring rotational bands. (Isomeric states in this region of nuclei were noticed already in ref. [5]).) A similar situation (fig. 20) occurs for ^{208}Pb (Z = 82, N = 126) but due to the very strong ground state shell effects, the isomeric state occurs at about 16 MeV of excitation probably with a very short half-life. Very low-lying

secondary minima occur for the two isotopes, ^{220,224}Ra, namely $Z = 88$, $N = 132$ and $Z = 88$, $N = 136$ exhibited in figs. 21 and 22. The secondary minima there occur at about 4 and 2 MeV of excitation, respectively. In particular the first case

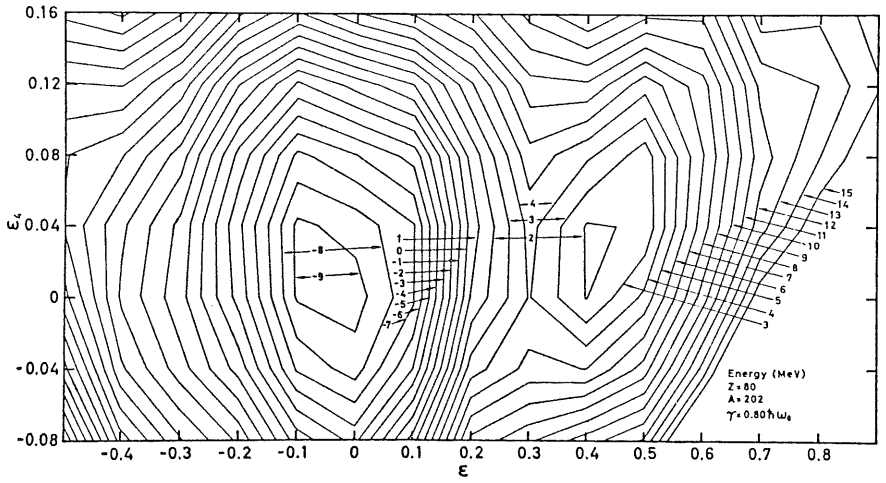

Fig. 19. Same as fig. 16 for ^{202}Hg.

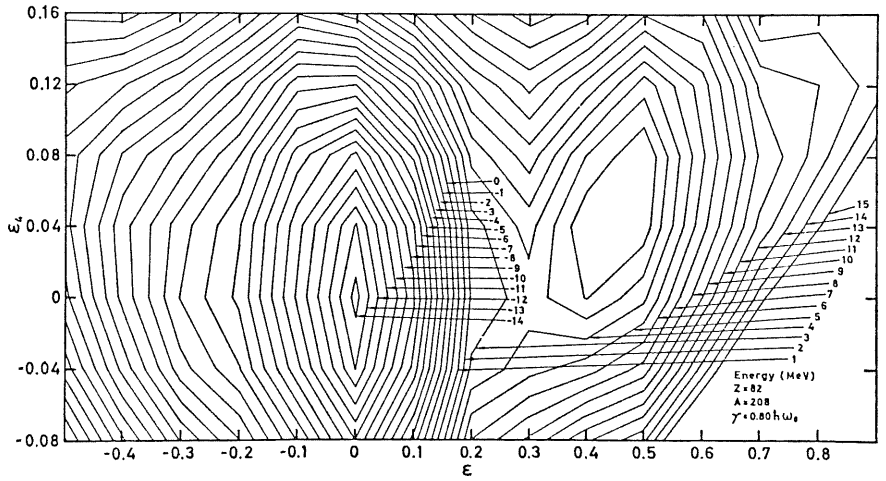

Fig. 20. Same as fig. 16 for ^{208}Pb.

shows a very substantial inner barrier and should be observable as an electromagnetic isomer. In none of the cases treated in this paragraph is fission a competitive mode of decay due to the dominance of the outer barrier. This in turn is due to the low x-values in this region of nuclei.

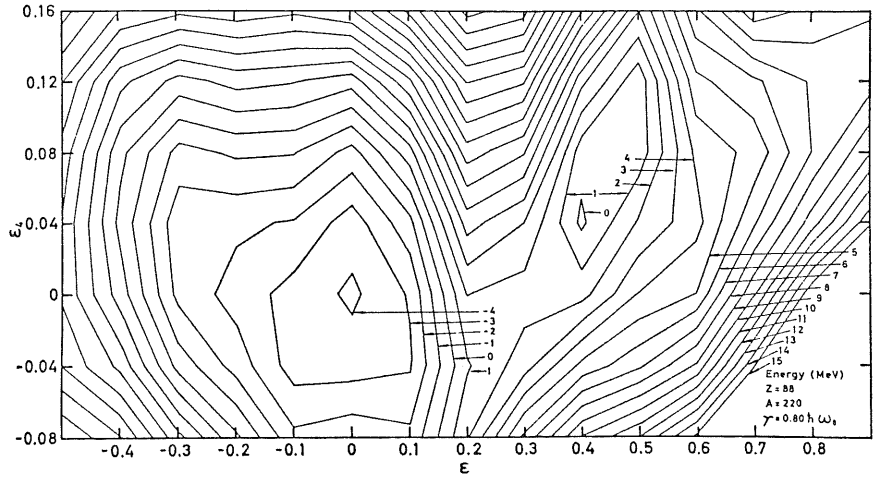

Fig. 21. Same as fig. 16 for ^{220}Ra.

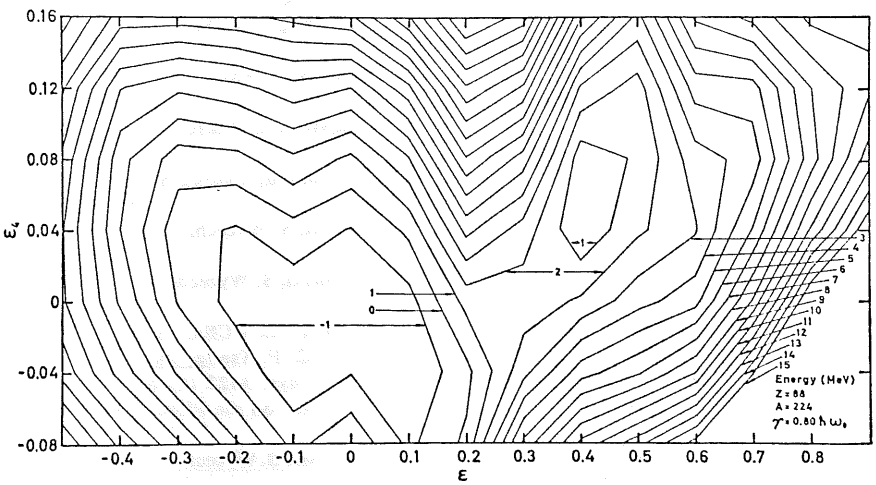

Fig. 22. Same as fig. 16 for ^{224}Ra.

7. Other possible cases of shape isomeric states

Shape isomeric states are also expected to occur in the superheavy nuclei region ($Z \sim 114$, $N \sim 184$) as is obvious from ref. [7]) and fig. 7 of this present paper. Here the secondary shell effect occurs at about the flat part of the liquid drop barrier. The two peak-character of the barrier is also in this region an apparent feature, although the second peak is somewhat lower than the first one.

A large number of new shape isomeric states are expected to arise in the odd-even and doubly odd nuclei due to the odd-nucleon effects. As the condition of conservation both of parity and of angular momentum along the axis of deformation has to be

upheld, the potential-energy surface is liable to exhibit an even larger number of local minima. The ones already present in the neighboring doubly even cases may be considerably deeper due to the effect of the odd-particle. This contention is well borne out by calculations presently being performed [21]).

The stimulating and constructive discussions with Dr. W. J. Swiatecki, and Dr. E. Cheifetz have been of great value for this work. We also gratefully acknowledge useful communications with Drs. S. G. Thompson, J. Borggreen, and S. Bjørnholm. The close cooperation with the Warsaw group of Drs. A. Sobiczewski, Z. Szymanski, and S. Wycech in our program is highly appreciated.

The friendly hospitality of the Nuclear Chemistry Division and its excellent publication services are gratefully acknowledged.

References

1) S. M. Polikanov, V. A. Druin, V. A. Karnaukov, V. L. Mikheev, A. A. Pleve, N. K. Skobolev, V. G. Subotin, G. M. Ter-Akopian and V. A. Fomichev, Exp. Theor. Phys. **42** (1962) 164; S. Bjørnholm, J. Borggreen, L. Westgaard and V. A. Karnaukov, Nucl. Phys. **A95** (1967) 513
2) G. N. Flerov and S. M. Polikanov, Compt. Rend. Congr. Int. Phys. Nucl. (Paris 1964) Vol. I, p. 407
3) N. Lark, G. Sletten, J. Pedersen, and S. Bjørnholm, Nucl. Phys. (1969) in press, and the references quoted therein
4) V. M. Strutinsky, Lysekil Symposium, 1966 (Almqvist and Wiksell, Stockholm, 1967), p. 629, and Ark. Fys. **36** (1967) 629
5) C. Gustafson, I. L. Lamm, B. Nilsson and S. G. Nilsson, Lysekil Symposium, 1966, op. cit., p. 613; Ark. Fys. **36** (1967) 613
6) S. G. Nilsson, J. R. Nix, A. Sobiczewski, Z. Szymanski, S. Wycech, C. Gustafson and P. Möller, Nucl. Phys. **A115** (1968) 545
7) S. G. Nilsson, C. F. Tsang, A. Sobiczewski, Z. Szymanski, S. Wycech, C. Gustafson, I. L. Lamm, P. Möller and B. Nilsson, Nucl. Phys. **A131** (1969) 1;
S. G. Nilsson, Lawrence Radiation Laboratory Report No. UCRL-18355-Rev. (Berkeley, Sept. 1968); cf. also S. G. Nilsson, S. G. Thompson and C. F. Tsang, Phys. Lett. **28B** (1969) 458
8) V. M. Strutinsky, Nucl. Phys. **A95** (1967) 420; Nucl. Phys. **A122** (1968) 1
9) V. M. Strutinsky and Zu. A. Muzychka, Proc. Int. Conf. on the Phys. of Heavy Ions, October, 1966, Vol. II, 51
10) P. Möller, S. G. Nilsson, A. Sobiczewski, Z. Szymanski and S. Wycech, Phys. Lett. **30B** (1969) 223
11) P. Möller and B. Nilsson, to be published
12) V. V. Pashkevich, Conf. Int. Symp. Nucl. Symp. Nucl. Structure, Dubna (1968) 94
13) W. D. Myers and W. J. Swiatecki, Lysekil Symposium, Sweden, 1966, (Almqvist and Wiksell, Stockholm, 1967), p. 393, and Ark. Fys. **36** (1967) 593
14) J. R. Nix, Further studies in the liquid-drop theory of nuclear fission, appendix, University of California Lawrence Radiation Laboratory Report UCRL-17958 (July 1968)
15) Yu. A. Muzychka, Phys. Lett. **28B** (1969) 539
16) A. Sobiczewski, Z. Szymanski, S. Wycech, S. G. Nilsson, J. R. Nix, C. F. Tsang, C. Gustafson, I. L. Lamm, P. Möller and B. Nilsson, Nucl. Phys. **A131** (1969) 67
17) Yu. P. Gangrskii, B. N. Markov, S. M. Polikanov, and H. Jungklaussen, Joint Institute of Nuclear Research R-2841, Dubna, 1966; and JETP Lett. **4** (1966) 289
18) Yu. P. Gangrskii, B. N. Markov, S. M. Polikanov, J. F. Harisov and H. Jungklaussen, Izv. Akad. Nauk USSR (phys. ser.) **32** (1968) 1644
19) H. R. Bowman, E. Cheifetz and R. C. Gatti, private communication
20) F. H. Ruddy and J. M. Alexander, to be published
21) G. Ohlén, S. G. Nilsson, C. Gustafson and P. Möller, Phys. Lett. **30B** (1969) 437
22) R. Vandenbosch and K. L. Wolf, University of Washington (Seattle), IAEA, 2nd Symp. on Phys. and Chem. of Fission, Vienna, 28 July–1 August 1969, Paper No. SM-122/110 (1969)